GEOPHYSICS, VOL 34, NO. 6 (DECEMBER 1969), P. 859–881, 20 FIGS.

VELOCITY SPECTRA—DIGITAL COMPUTER DERIVATION AND APPLICATIONS OF VELOCITY FUNCTIONS†

M. TURHAN TANER* AND FULTON KOEHLER‡

Multifold ground coverage by seismic techniques such as the common reflection point method provides a multiplicity of wave travel path information which allows direct determination of root-mean-square velocities associated with such paths. Hyperbolic searches for semblance among appropriately gathered arrays of traces form the basis upon which velocities are estimated. Measured semblances are presented as a velocity spectral display. Interpretation of this information can give velocities with meaningful accuracy for primary as well as multiple events. In addition, the velocity data can help correctly label events. This paper outlines the fundamental principles for calculating velocity spectra displays. Examples are included which demonstrate the depth and detail of geological information which may be obtained from the interpretation of such displays.

MOTIVATIONS FOR AND HISTORICAL BACKGROUNDS OF VELOCITY ANALYSIS

Proper indentification of primary reflections amidst a background of noise and energy from various multiple reflections was a major problem when all seismic work was single coverage and is still a problem in the common reflection point multifold coverage method. Many analog and digital techniques have been developed to reduce this undesirable interference and have been utilized with varying degrees of success. Time-varying inverse filtering and common reflection point techniques are among the most effective procedures. See for instance Mayne (1962) and Courtier and Mendenhall (1967).

The objective of improved signal-to-noise ratio and attenuation of multiples utilizing the CRP method can be accomplished only by applying the proper time corrections to the seismic data, so that the primary reflection signals will be moved in-phase and stacked properly. It is first necessary, therefore, to determine corrections for all primary reflections for all the traces (with different shot-to-geophone distances) which will be stacked into a single trace.

This work develops and discusses the velocity spectral display as a powerful tool for identifying primary reflections and stacking velocities. Information relevant to lithology is also shown to be present by careful study of these displays. Underlying the method is the well-established principle of employing a correlation-like technique upon an assemblage of seismic traces which contain redundant information so that an improved estimate of some desired quantity may be made. Rieber (1936), Trorey (1961), Picon and Utzmann (1962), and Simpson (1967) are among the authors who have also recognized and used this idea. In fact, the velocity analysis of Schneider and Backus (1968), which was developed contemporaneously with our method, also made use of these fundamentals.

THE VELOCITY SPECTRA DISPLAY, CONSTRUCTION

In the past, time corrections have been estimated from previously measured nearby well velocities utilizing simple straight-ray or curved-ray methods, and resulting misalignments were corrected by applying residual normal moveout corrections. This procedure is somewhat unsatisfactory because it is time consuming and, since the data is handled more than once, it is costly. It becomes more unsatisfactory when there is no

† Presented at the 37th Annual International SEG Meeting, Oklahoma City, November 2, 1967. Manuscript received by the Editor December 17, 1968; revised manuscript received August 1, 1969.

* Seismic Computing Corp., Houston, Texas 77036.

‡ Seismic Computing Corp., Houston, Texas 77036, and University of Minnesota, Minneapolis, Minnesota 55455.

DOI:10.1190/1.1440058

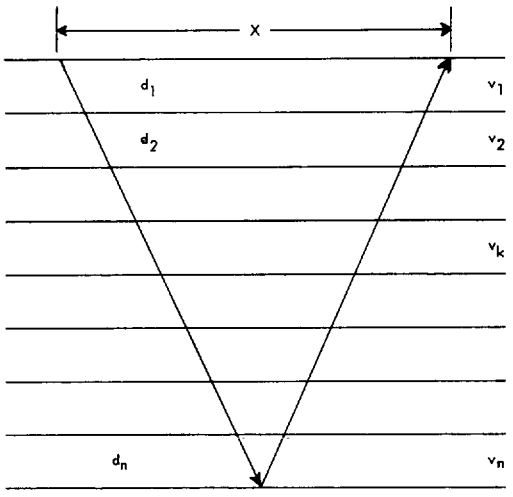

FIG. 1. Straight ray analysis in horizontally layered medium.

well data available. In any case, the time corrections from known data are generally generated from the simple case of horizontally layered media and effects of dipping beds are not considered.

Let us now consider a horizontally layered medium (Figure 1) where,

v_k = interval velocity at kth layer,
d_k = thickness of kth layer,
t_k = two-way traveltime within the kth layer, $t_k = 2d_k/v_k$,
X = horizontal distance between the energy source and detecting device.
$T_{0,n}$ = two-way vertical traveltime to the base of nth layer

$$T_{0,n} = \sum_{k=1}^{n} t_k = 2 \sum_{k=1}^{n} \frac{d_k}{v_k}, \qquad (1)$$

$V_{a,n}$ = average velocity to the base of nth layer

$$V_{a,n} = \frac{\sum_{k=1}^{n} v_k t_k}{T_{0,n}} = \frac{2 \sum_{k=1}^{n} d_k}{T_{0,n}}, \qquad (2)$$

$T_{x,n}$ = arrival time of a reflection from the base of nth layer at X distance.

Now, if we assume that the wavefront is traveling along the shortest (distance) path between the energy source, reflector, and geophone, total traveltime, which we will call arrival time, $T_{x,n}$ is given by the familiar relationship

$$T_{x,n}^2 = T_{0,n}^2 + \frac{X^2}{V_{a,n}^2}. \qquad (3)$$

However, we know that the wavefront is traveling along the shortest time path, in accordance with Fermat's principle, hence the arrival time will be given by the infinite series of the form (Figure 2)

$$T_{x,n}^2 = c_1 + c_2 X^2 + c_3 X^4 + c_4 X^6 + \cdots \qquad (4)$$

where the coefficients $c_1, c_2, \cdots$, depend on layer thicknesses $d_1, d_2, \cdots, d_n$, and the interval velocities $v_1, v_2, \cdots, v_n$. Derivation of equation (4) is presented in Appendix A, and it is in accordance with Snell's law. Studies have shown that, for the X distances generally encountered in practice, the first two terms of equation (4) give an accuracy of about 2 percent which is adequate for seismic exploration purposes. Therefore, we can neglect all the terms containing higher powers of X^2, and simplify the expression to,

$$T_{x,n}^2 = c_1 + c_2 X^2, \qquad (5)$$

where

$$c_1 = \left(\sum_{k=1}^{n} t_k \right)^2 = T_{0,n}^2 \qquad (6)$$

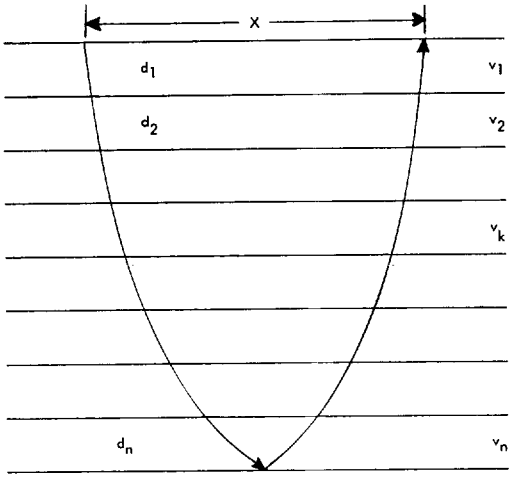

FIG. 2. Snell's law ray analysis in horizontally layered medium.

$$c_2 = \frac{\sum_{k=1}^{n} t_k}{\sum_{k=1}^{n} t_k v_k^2} \equiv \frac{1}{\overline{V}_n^2}, \quad \text{or,}$$

$$\overline{V}_n^2 = \frac{\sum_{k=1}^{n} v_k^2 t_k}{T_{0,n}}. \tag{7}$$

Therefore, equation 5 becomes,

$$T_{x,n}^2 = T_{0,n}^2 + \frac{X^2}{\overline{V}_n^2} \tag{8}$$

which is very similar to equation (3), with the notable difference that, instead of average velocity $V_{a,n}$, we are using $\overline{V}_n$, as defined by equation (7). This apparent velocity is the same one as given in a formula by Dix (1955), and represents the time-weighted, mean-square velocity. In order to differentiate it from the linear average velocity, we will call this the rms (root-mean-square) velocity. This expression suggests that, in the areas where the beds have gentle dips, the time corrections could be computed fairly accurately by

$$\Delta T_n = \sqrt{T_{0,n}^2 + \frac{X^2}{\overline{V}_n^2}} - T_{0,n}, \tag{9}$$

where

$$\Delta T_n = T_{x,n} - T_{0,n}. \tag{10}$$

When we consider the problem for the general case of arbitrarily dipping beds, it becomes practically impossible to obtain an expression similar to equation (4) that would give the explicit relation between time and distance. However, we could obtain this relation by studying mathematical models and ray tracing using Snell's law. Figure 3 shows an example of the model study where CDP traces for a horizontally layered case have been simulated. Observed and computed arrival times, distances, and rms and average velocities are tabulated for comparison. It should be noted that the average velocity is lower than the rms velocity in all cases.

Single coverage record simulation for dipping interfaces is shown in Figure 4. In this example, the shotpoint is assumed to be at the center of the spread. Time-distance relations are still nearly hyperbolic, however, the curves are translated in the updip direction. Figure 4 also contains computed raypaths for a few typical geophone locations. There is a unique and most important raypath among all of these, that is, the one for which shotpoint and recording geophone are in the same location, and the travel path is perpendicular to the reflector so that incident and reflected raypaths become the same. We will call this path the

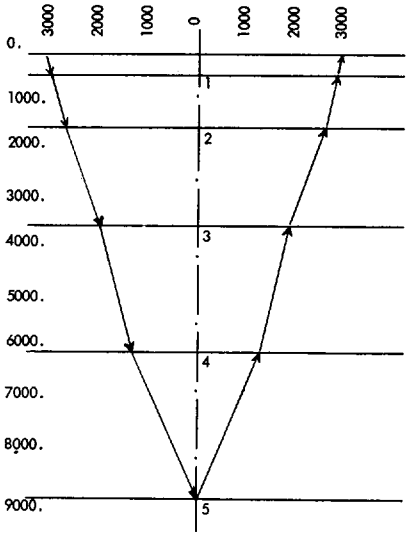

$d_1 = 400'$ $V_1 = 5000'/\text{sec.}$
$d_2 = 1000'$ $V_2 = 6000'/\text{sec.}$
$V_{a2} = 5676$ $\overline{V}_2 = 5695$
$d_3 = 2000'$ $V_3 = 8000'/\text{sec.}$
$V_{a3} = 6846$ $\overline{V}_3 = 6951$
$d_4 = 2500'$ $V_4 = 6500'/\text{sec.}$
$V_{a4} = 6695$ $\overline{V}_4 = 6758$
$d_5 = 3000'$ $V_5 = 10000'/\text{sec.}$
$V_{a5} = 7534$ $\overline{V}_5 = 7712$

COMPUTED VS. ESTIMATED* $T_{x,n}$

No.	REFLECTOR DISTANCE (ft.) 0	1800	3000	4200	6000	
1	.1600	.3940	.6210	.8551	1.2105	Comp.
	.1600	.3940	.6210	.8551	1.2105	Est.
2	.493	.586	.721	.884	1.154	
	.493	.586	.722	.887	1.163	
3	.993	1.027	1.083	1.161	1.311	
	.993	1.027	1.083	1.163	1.316	
4	1.763	1.783	1.818	1.869	1.973	
	1.763	1.783	1.818	1.869	1.974	
5	2.363	2.374	2.394	2.424	2.487	
	2.363	2.374	2.394	2.424	2.487	

(*) $T_x^2 = T_o^2 + \frac{X^2}{\overline{V}_n^2}$

Where $\overline{V}_n$ = R.M.S. Velocity

FIG. 3. Horizontally layered model study.

DOI:10.1190/1.1440058

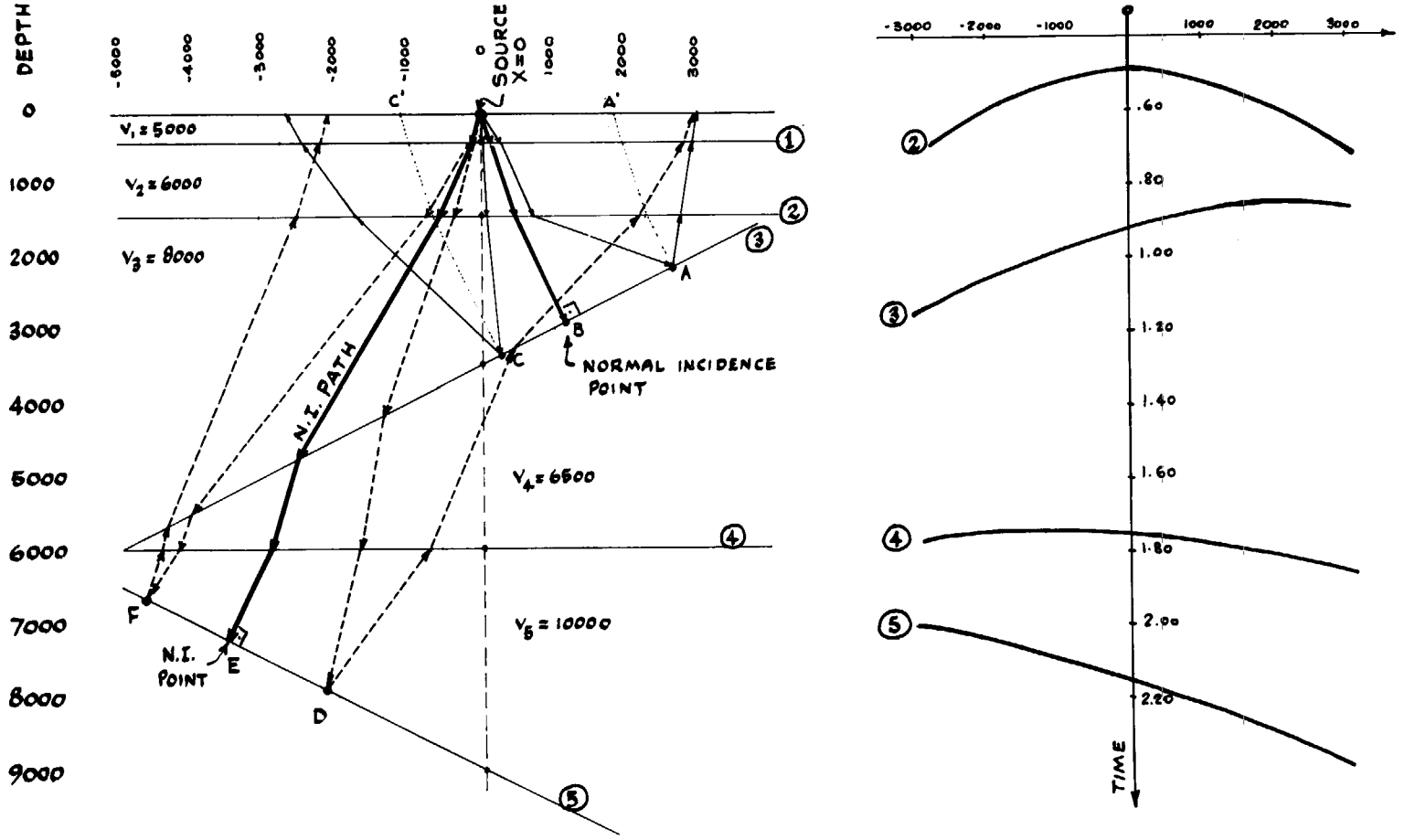

FIG. 4. Single coverage model with dipping reflectors—depth and CRP time section.

DOI:10.1190/1.1440058

normal incidence path (NIP) and the time taken to travel this path (from shot to reflector to geophone) the normal incidence time (NIT).

The time correction (ΔT_n) in the case of single coverage records is the time difference between the total traveltime (from shot to a particular reflection point to the geophone) and normal incidence time for that particular reflection point. By applying a time correction to a given trace, we are generating a new trace whose shot and recording positions coincide at the ground position of the normal incidence path going through the reflection point.

Now let us look at the common-depth-point simulation as shown on Figure 5. These travel paths are generated by assuming shot and recording locations are kept symmetrical with respect to the ground position. In this example we are keeping all conditions the same as in the previous example with one exception. In this case the previous shot location now becomes the common ground point on which the stack is based.

Experiments using differing dips and interval velocities indicated that arrival time-distance relations remain nearly hyperbolic. This has been further verified by the closeness of least-squares fit hyperbolas to synthetically generated time-distance values. If we assume that the parameters of these hyperbolas are similar to those as shown in equations (5) and (8), we would then define the values of the apparent velocities observed from common reflection point traces. Investigation has also shown that, if we keep all the parameters the same, increasing dips produce increased apparent velocities or flatter time-distance curves. One interesting and important point is that the travel path between the shot and recording with respect to any reflecting bed is reversible. That is, if we exchange the shot and recording position, the travel path (although reversed) and traveltime stay the same. Therefore, the time-distance relation represents a symmetric curve and its apex is always at $X=0$. Furthermore, the arrival time at the apex (minimum arrival time) is equal to the normal incidence time at the common ground point. The time correction (ΔT_n) in the case of common depth point traces, is the time difference between the total traveltime for a given shot-geophone position and the normal incidence time at the common ground point.

By applying time corrections (NMO) to the traces obtained with shooting and recording symmetrically disposed about a ground point, we are actually simulating a new set of traces that theoretically were shot and recorded at the same place, the common ground point. This time correction is different from the time correction applied to the single coverage records, and the main confusion about time corrections for stacked data stems from misunderstanding this difference (see Nugent, 1967). Since the time-distance relations are still nearly hyperbolic, records should be stacked just as properly in the dipping bed cases as they would be stacked in horizontal bed areas, provided that the parameters of the hyperbola are determined properly. This could be done without the remedial procedure of residual moveout correction.

One of the generally practiced methods for determining corrections is the T^2 versus X^2 study of common reflection point traces. However, this normal-visual method is somewhat limited by the seismic interpreter's ability to recognize and analyze visible strong reflectors. If we display the input traces to a common reflection point gather according to their X distances (Figure 6), reflections coming from a common reflector should appear along a particular hyperbola. Also, each unique set of reflections would have a normal incidence time and an apparent rms velocity (apparent owing to the assumption of horizontal layering and neglect of dip).

This display which we are used to observing, shows the reflected energy as a function of two variables, time and distance. Hence, mathematically we are looking at a reflection energy surface over the time-distance domain. It is, therefore, possible to display this reflected energy in a more convenient two-variable domain, normal incidence time—rms velocity. This can be accomplished by transforming the reflected energy from one domain (energy as a function of time and distance) into another (energy as a function of normal incidence time and apparent rms velocity).

Details of the transformation can, of course, vary; however, if a process generically related to correlation with a suite of curves is used, the output may be referred to as a spectrum. We note that the familiar Fourier calculation is based on correlation with sinusoids. Clearly then the search for a velocity with a constant normal

DOI:10.1190/1.1440058

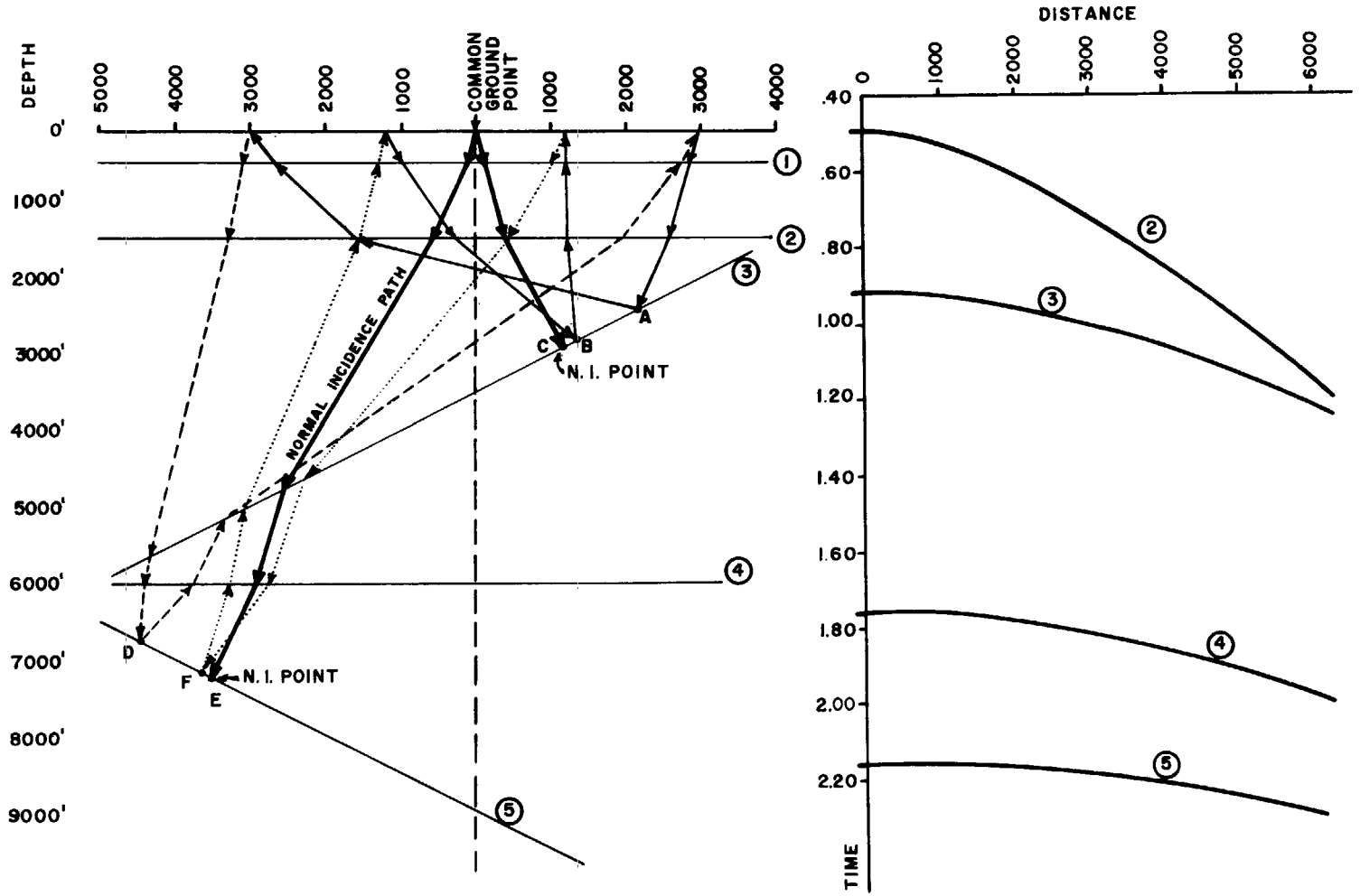

FIG. 5. Common reflection point model with dipping reflectors.

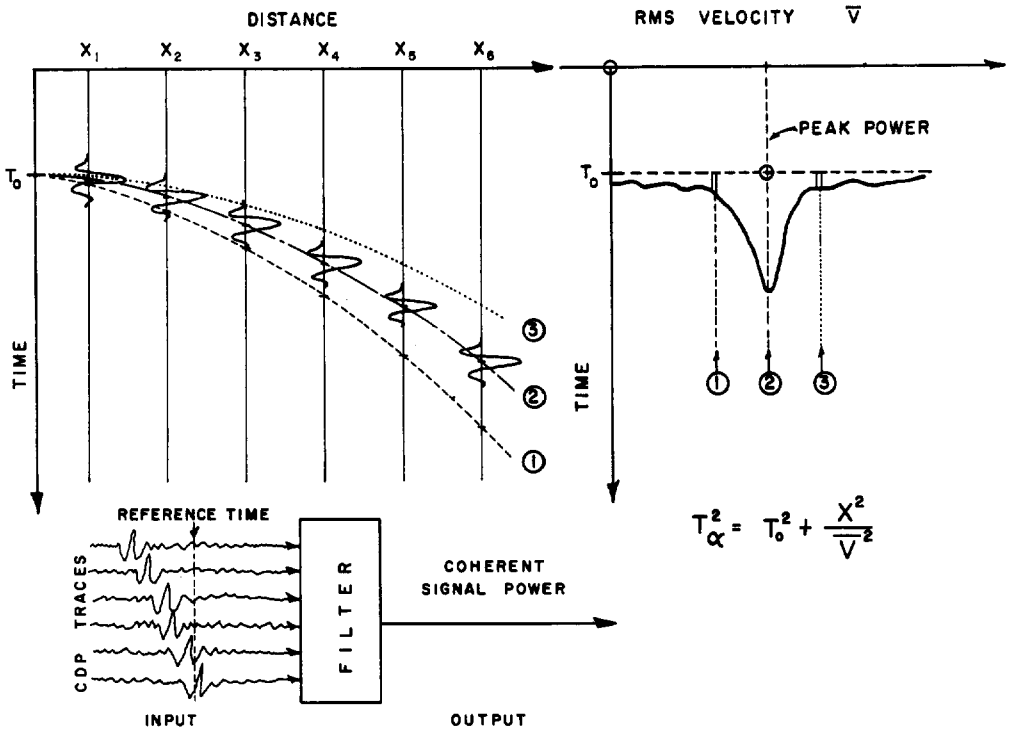

FIG. 6. Trace gather for a velocity search.

incidence time gives a velocity spectrum and the display summarizing such searches for all normal incidence times constitutes velocity spectra.

The transformation must serve to measure the power of reflections arriving according to various paths as given by equation (8). For this purpose, a specially designed multichannel filter was utilized. This filter, a semblance filter, is a normalized crosscorrelation function (see Appendix B) and measures the common signal power over the channels according to the specified lag pattern. A schematic diagram of this filter is shown on Figure 6. After the alignment of the input data with respect to a given hyperbolic delay pattern, a digital filter is computed for each trace that would selectively pass events common to all traces. Then, these are stacked together to give the best estimate of the input signal. The power of this estimate is then computed by summing the amplitude squares within a specified time gate around the reference time and this power is then displayed on the velocity spectra. Computation of power spectra for a given set of traces is done on a grid pattern. First, a reference time $T_{0,n}$ is chosen. The time is kept constant and $\overline{V}_n$ is then varied at regular intervals between a minimum and maximum $\overline{V}$ for a given area. Each set of $T_{0,n}$ and $\overline{V}_n$ will give a particular hyperbolic pattern. Each trace is displaced an amount corresponding to the X distance, passed through the semblance filter, and output power is displayed with respect to its corresponding $T_{0,n}$ and $\overline{V}_n$ values as shown on Figure 6. Peaks on the spectrum thus indicate the arrival of reflected energy at this particular $T_{0,n}$ time with an apparent velocity indicated by the corresponding $\overline{V}$ coordinate.

To generate a velocity spectrum then, we sweep the traces with various hyperbolas but always keep the apex at one point, $X=0$. After examining a predetermined range of velocities, a new $T_{0,n}$ is chosen at a time equal to half the time gate down the traces. Another sweep of predetermined velocities is made at this new $T_{0,n}$ and results in all reflections being analyzed. In other words, a complete spectrum (velocity sweep) is computed at constant intervals down the record. This procedure starts at a given time and is repeated

down the record until the desired final analysis time is reached.

Figure 7 shows a typical velocity spectra display computed from 0.200 sec to 4.000 sec for velocities varying from 5000 ft/sec to 10,000 ft/sec at 100 ft/sec intervals. This is generated from 24 traces (shown on the right side of the figure) composed of 4 sets of 6 traces from 4 adjacent common ground points. Increasing power is shown as displacement in the direction of increasing time. Velocity spectra are interpreted in a manner similar to the interpretation of conventional seismic traces. In this case the velocity function is obtained by connecting the interpreted primary energy arrivals as indicated on the figure. These spectra also show some multiple energy around 3.2 to 3.8 sec with 7000 to 8000 ft/sec velocity. Since the spectra are computed for overlapping time gates and very close velocity intervals, the final display will contain the results of analysis of all the reflections, primaries, multiples, and other types of coherent energy.

THE VELOCITY SPECTRA DISPLAY, USES

Several uses of the velocity spectra display suggest themselves.

Velocity spectra displays help to determine the velocity function needed for optimum stacking. In order to determine this, the spectra are interpreted and primary reflections are identified. If the chosen velocity function goes through the primary reflections where they appear on the spectra, we are assured that they will be stacked properly and will appear on the final stacked section.

They may be used to check the final section against any procedural, interpretational, or computational error. For instance, if for some reason a reflection chosen as a good primary reflection on the velocity spectra display is not found on the stacked section and the 100 percent section shows improper time correction, this is a good indication that the spectra were interpreted improperly or some other error occurred during the processing. Instead of arbitrarily applying a residual move-out correction, spectra can be reinterpreted and all of the input data rechecked.

They aid in determining the effect of multiple interference. Since velocity spectra encompass all reflections, it is, in many cases, possible to determine the timing, order, apparent velocity, and relative power of multiples. These, in comparison with the primary reflections, will give us a good indication of the multiple content of the stacked section. Looking back at Figure 7, we can conclude that the section down to 2.8 sec will consist primarily of strong primary reflections, and the possible blurring effect around 3.4 to 3.8 sec is due to strong multiples.

The velocity spectra can be used to determine two-way normal incidence time and rms (apparent) velocity of major reflectors for later use in interpretation. We can estimate the interval velocities between major reflectors by the expression,

$$v_n^2 = \frac{\overline{V}_n^2 T_{0,n} - \overline{V}_{n-1}^2 T_{0,n-1}}{T_{0,n} - T_{0,n-1}} . \qquad (11)$$

Extensive experience, such as Cook's (1967), has shown that in areas of gentle dips (less than 5 degrees), equation (11) gives interval velocities 2 percent to 3 percent higher than actually measured in well-velocity surveys and can be used in the initial interpretation stage. These values, normal incidence time and rms velocities, from different velocity spectral analyses are later used to compute more precise interval velocities, reflection depths, layer thickness, dip and other parameters for two or three dimensional migration.

They can be used to obtain stratigraphic and structural information. Experience over the past two years has shown that much stratigraphic information is also contained on the spectra. Changes of character of primaries on velocity spectra displays within a given area serve as a good indicator that changes have taken place in the stratigraphy. Figure 8 shows a velocity spectra display in which primary energy appears to stop at about 2.24 sec. Below this line we see a series of multiples that persist to about 4.0 sec where another strong reflection with about a 9200 ft/sec velocity appears. This disappearance of primary reflections between 2.24 and 4.0 sec is due to a large shale body which is known to exist in this particular area.

ILLUSTRATIONS OF THE USE OF VELOCITY SPECTRA

Figure 9 shows a stacked section of an experimental marine Vibroseis line from offshore Louisiana and further shows the kind of information given by velocity spectra. Figure 10 shows three velocity spectra displays computed along

DOI:10.1190/1.1440058

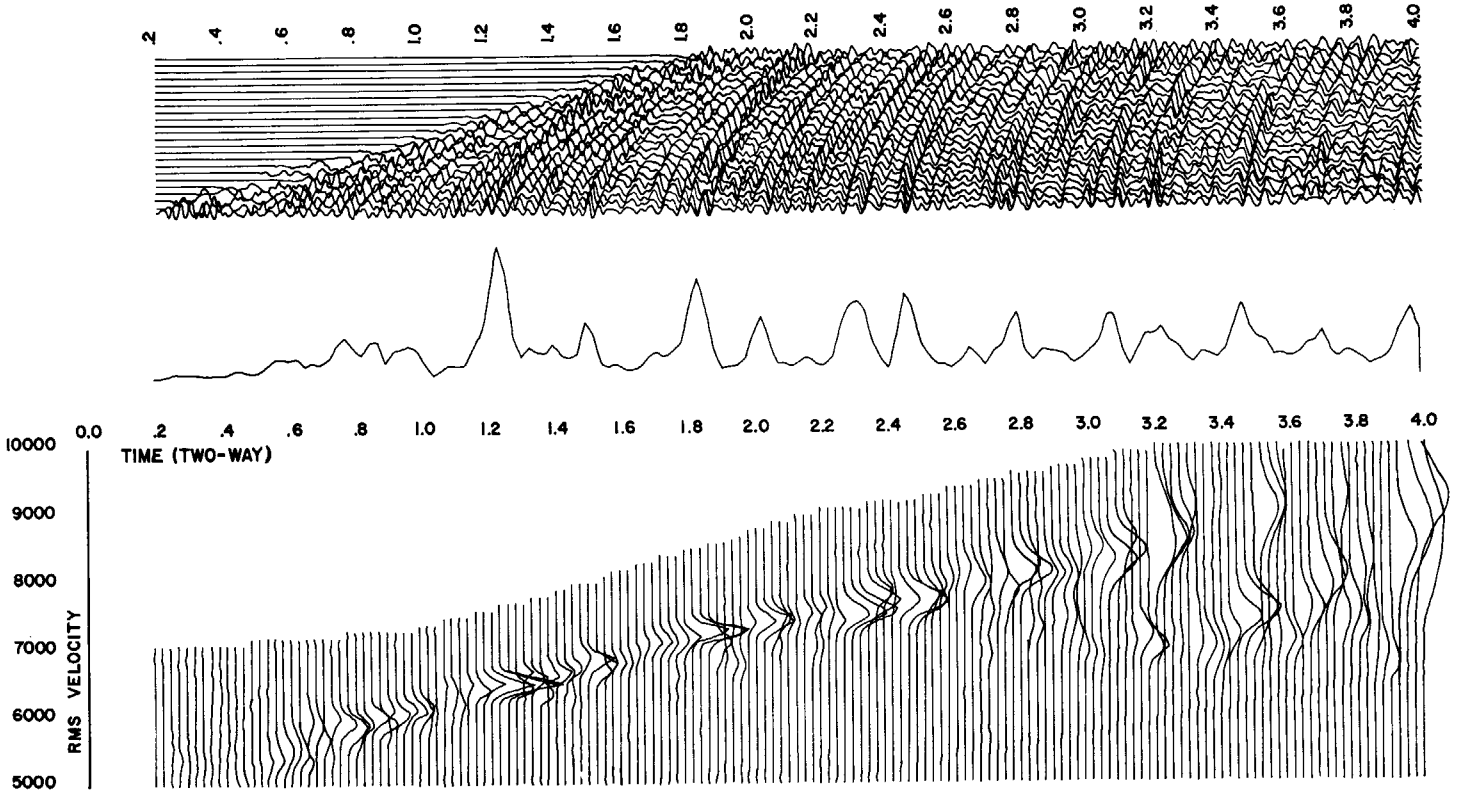

FIG. 7. Typical velocity spectra display.

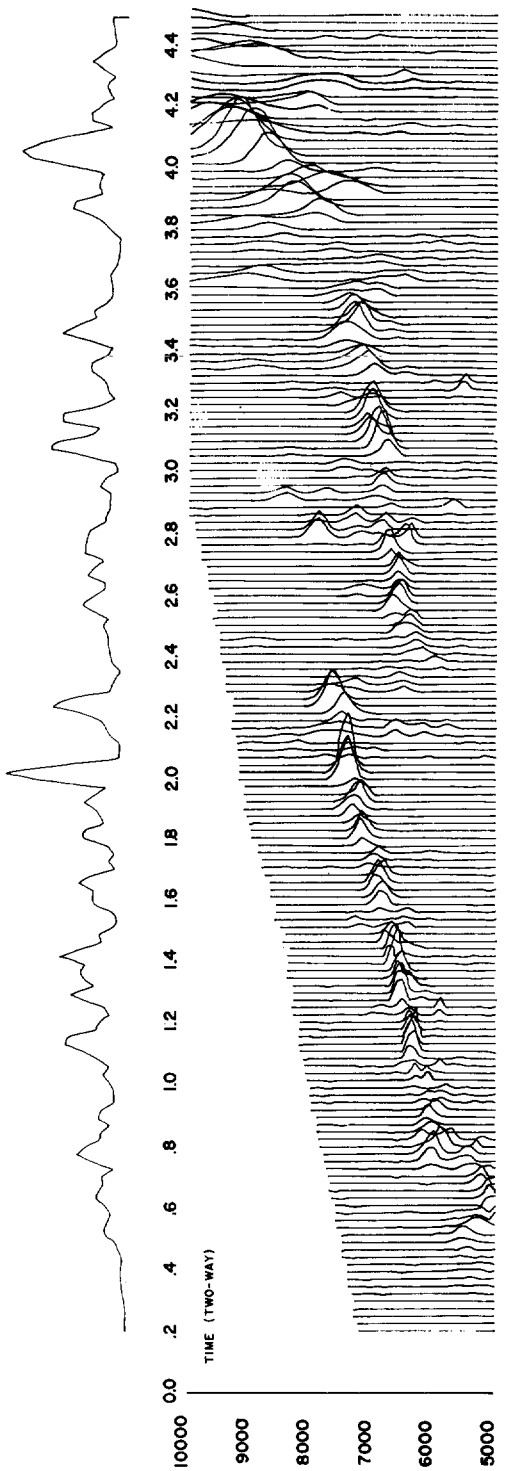

FIG. 8. Velocity spectra display showing reflection loss caused by shale body.

this line at three of the locations indicated on Figure 9. These spectra are plotted with the same time scale as the final sections so that geophysicists can lay the spectra on the section as an aid in interpretation. These spectra are also used in the computation of time-varying-multichannel filters that pass only the desired primary reflections and attenuate multiple reflections and random noise. Such a section is shown in Figure 11. Spectra in Figure 10 indicate that the section contains mostly primary energies down to 2.6 to 3.2 sec, and also shows a gentle velocity gradient. For example, the rms velocity at 1.4 sec on the west side of the section is 6400 ft/sec, on the east side it is 5900 ft/sec. A single velocity function would, therefore, result in under or over-corrected records.

In actual practice time corrections between spectra locations are interpolated from the two nearby spectra. This allows us to follow the velocity gradient closely without an abrupt change of velocity functions. Character correlation on the spectra also sometimes help in the structural interpretation. For example, the reflection at 3.16 sec on the spectra display at SP 6 has a character similar to that of the reflection at 3.04 sec on the spectra at SP 73. Comparing this with the section, we see that both are coming from the same interface. Moving over to the spectra at SP 233, we see that similar character appears at 2.60 sec.

Figure 12 shows a velocity spectra display computed on land data from South Texas. Initially, the reflection around 2.0 sec was thought to be the deepest primary in the area. The spectra show some additional primaries between 2.0 and 3.0 sec which were identified as sand layers in a later drilled well.

North Sea data generally contain very strong reflections, as well as strong surface and peg-leg multiples. Figure 13 shows various spectra from the North Sea. In some instances, where strong multiples are present, it is difficult to see or identify the primary energy below the strong reflector. After these multiples are identified, they are removed from the traces and new (multiples eliminated) spectra are computed. An example of this application is shown in Figure 14. Eliminations of reflections (multiple or primary) is accomplished with the same type multichannel filters used in spectra computation. However,

DOI:10.1190/1.1440058

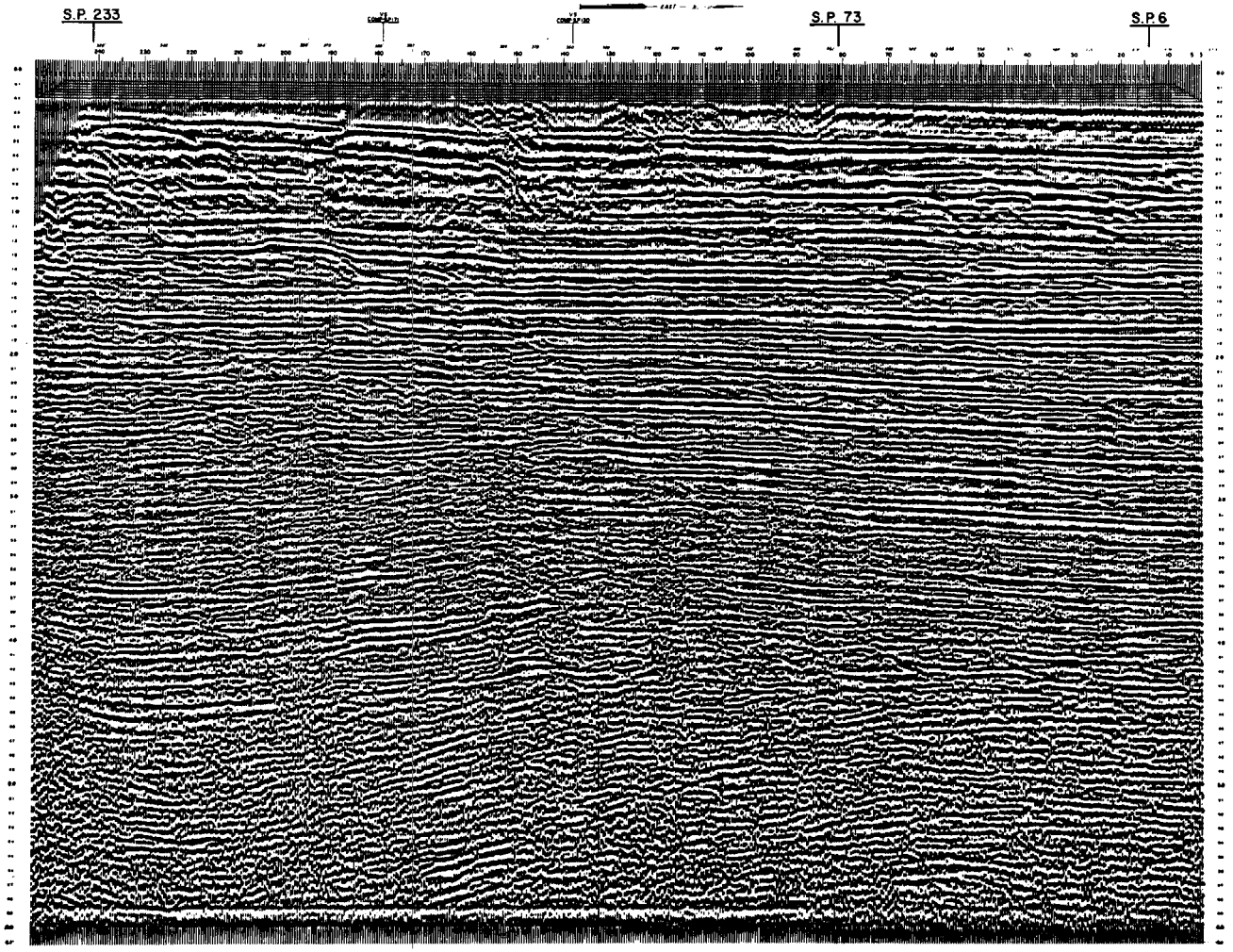

FIG. 9. Stacked section using primary velocities derived from spectral display (Offshore Louisiana).

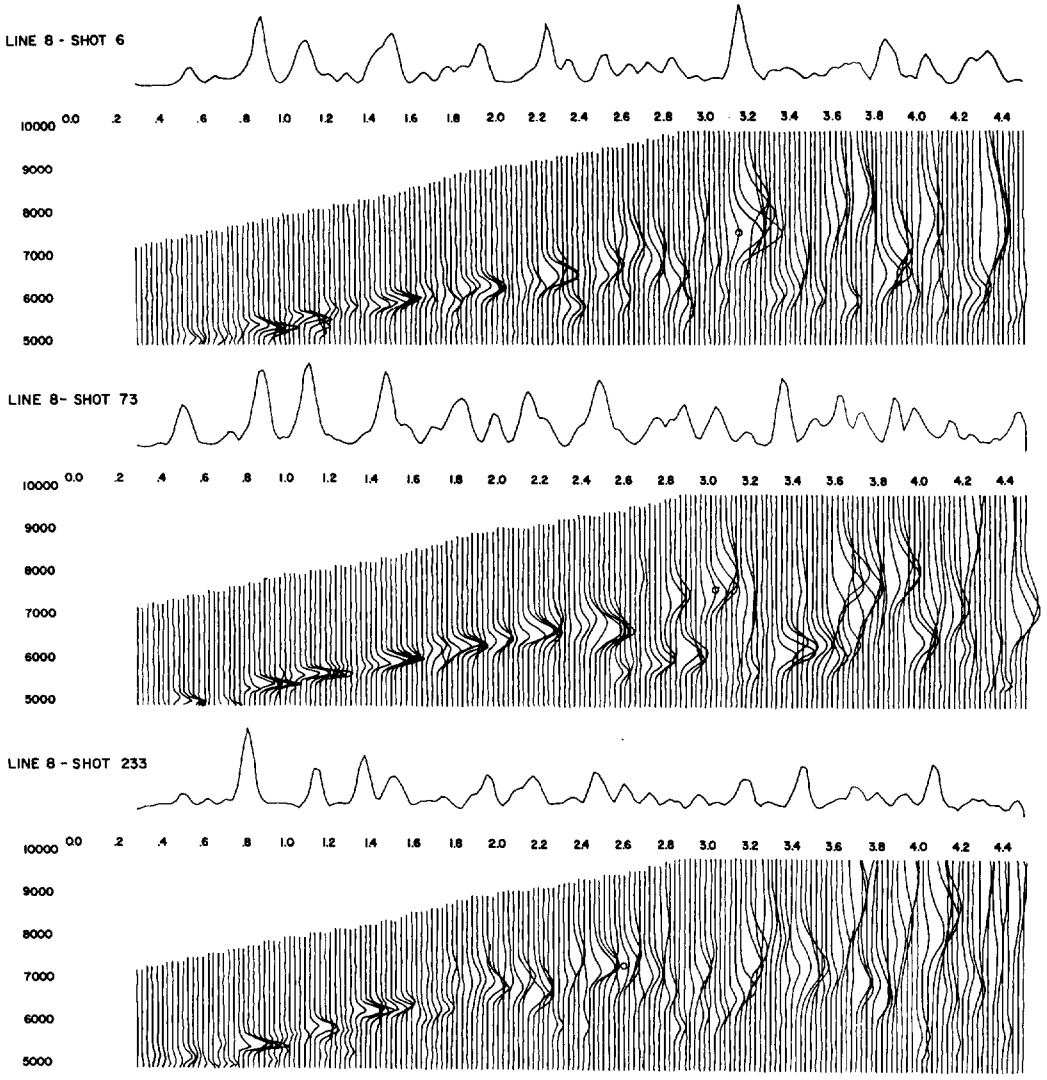

FIG. 10. Spectral displays illustrating continuity of reflections and character in spectral domain.

these filters are in this case modified to attenuate the semblant energy arriving at a given time and with a given velocity.

One of the most difficult interpretational problems is the interpretation of a velocity inversion. Figure 15 shows three spectra displays computed in an area with such an inversion, whose existence was later verified by drilling. The trends of the spectra warn us of the existence of a possible inversion. Interpretation of deeper reflections becomes more difficult owing to the existence of various multiples in the primary energy zone.

During the past two years, velocity spectra displays have been computed on data from all parts of the world and for all types of energy sources. Figure 16 shows a set of spectra computed from gas gun records. Figure 17 shows spectra computed from marine Vibroseis records in the deep sea.

VELOCITY SPECTRA FOR EARTH MODELS

Earlier in the paper it was shown that arrival times and apparent velocities from single or

DOI:10.1190/1.1440058

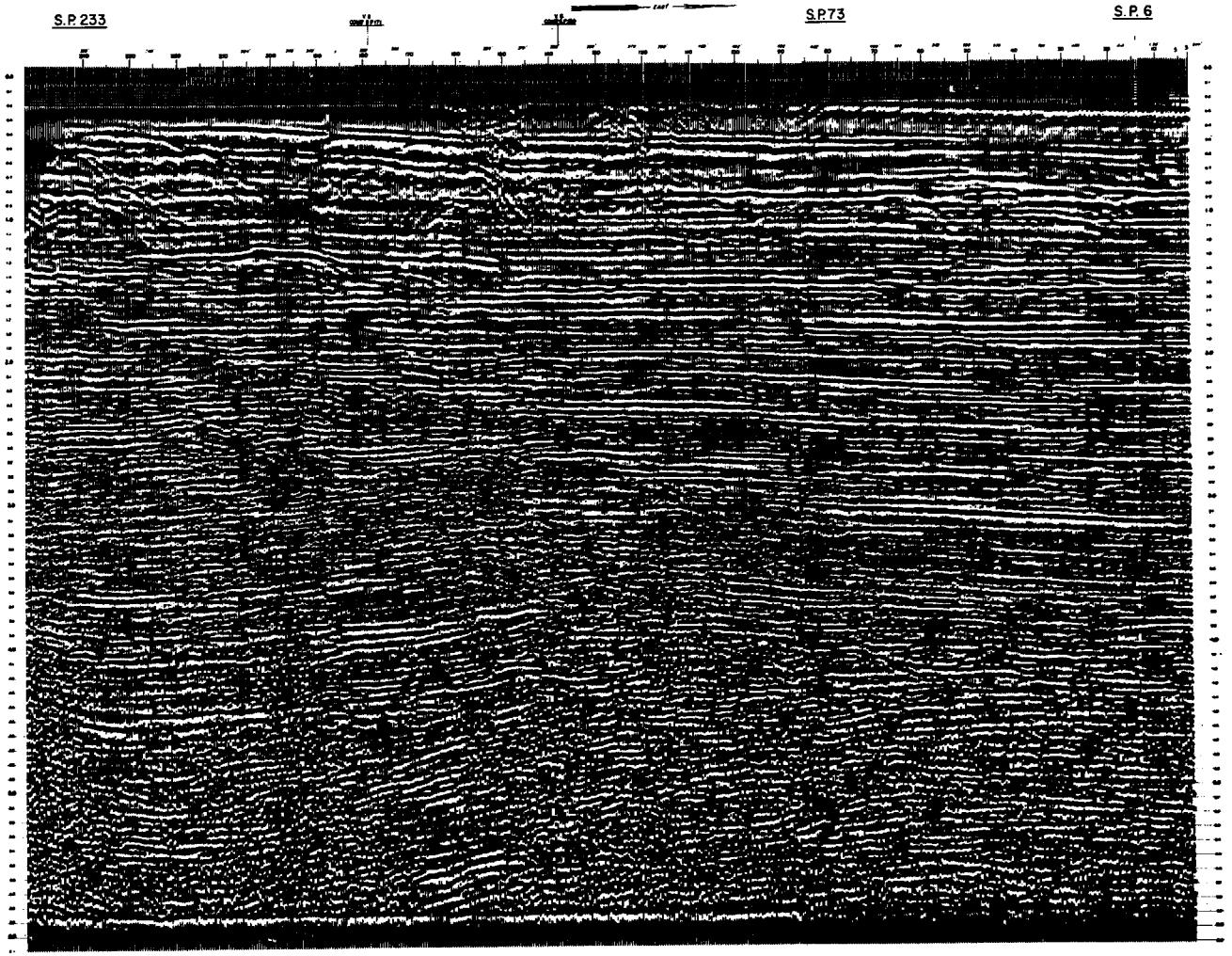

FIG. 11. Seis/Stack[1] section (Offshore Louisiana).

[1] Seismic Computing Corp. Trademark.

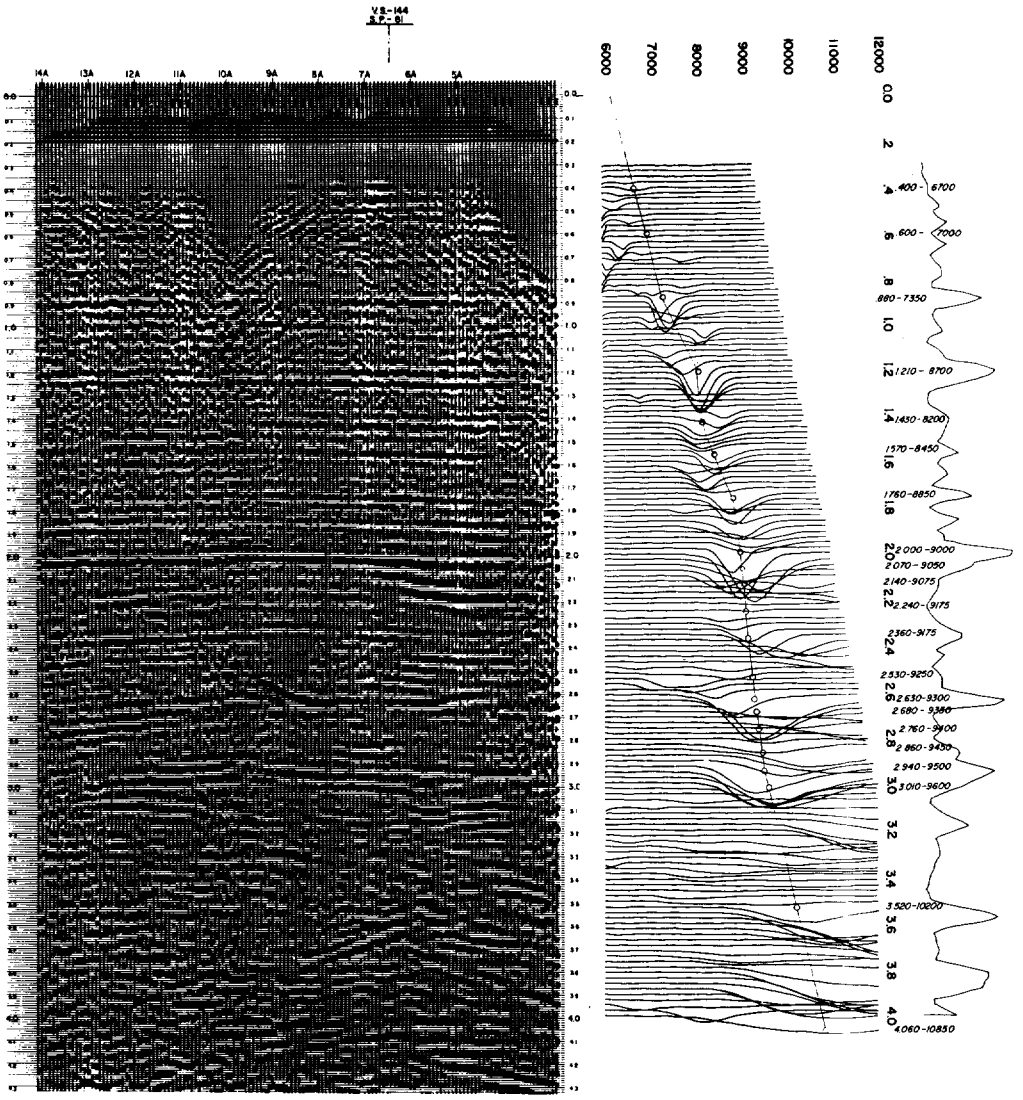

FIG. 12. Spectral display and section for land data (South Texas).

multiple coverage records could be computed by generating a simulated mathematical model from known interval velocities, dips, and layer thicknesses. Conversely, it is also possible to compute the interval velocities, dips, and layer thicknesses by generating a model for which the arrival times and apparent velocities are the same as of those observed from field records. This method is presently used in dip, depth, and interval velocity computation from velocity spectra and a sample output of such a computation is shown on Figure 18. This procedure is programmed so that the computer builds the model one layer at a time, and by iteration it minimizes the difference between the observed and computed values of arrival times and apparent rms velocities. The iteration procedure is terminated when the differences are less than a desired value. The accuracies of these computed dips, depths, and interval velocities are completely dependent on the accuracies of the observed arrival times and apparent velocities on the velocity spectra.

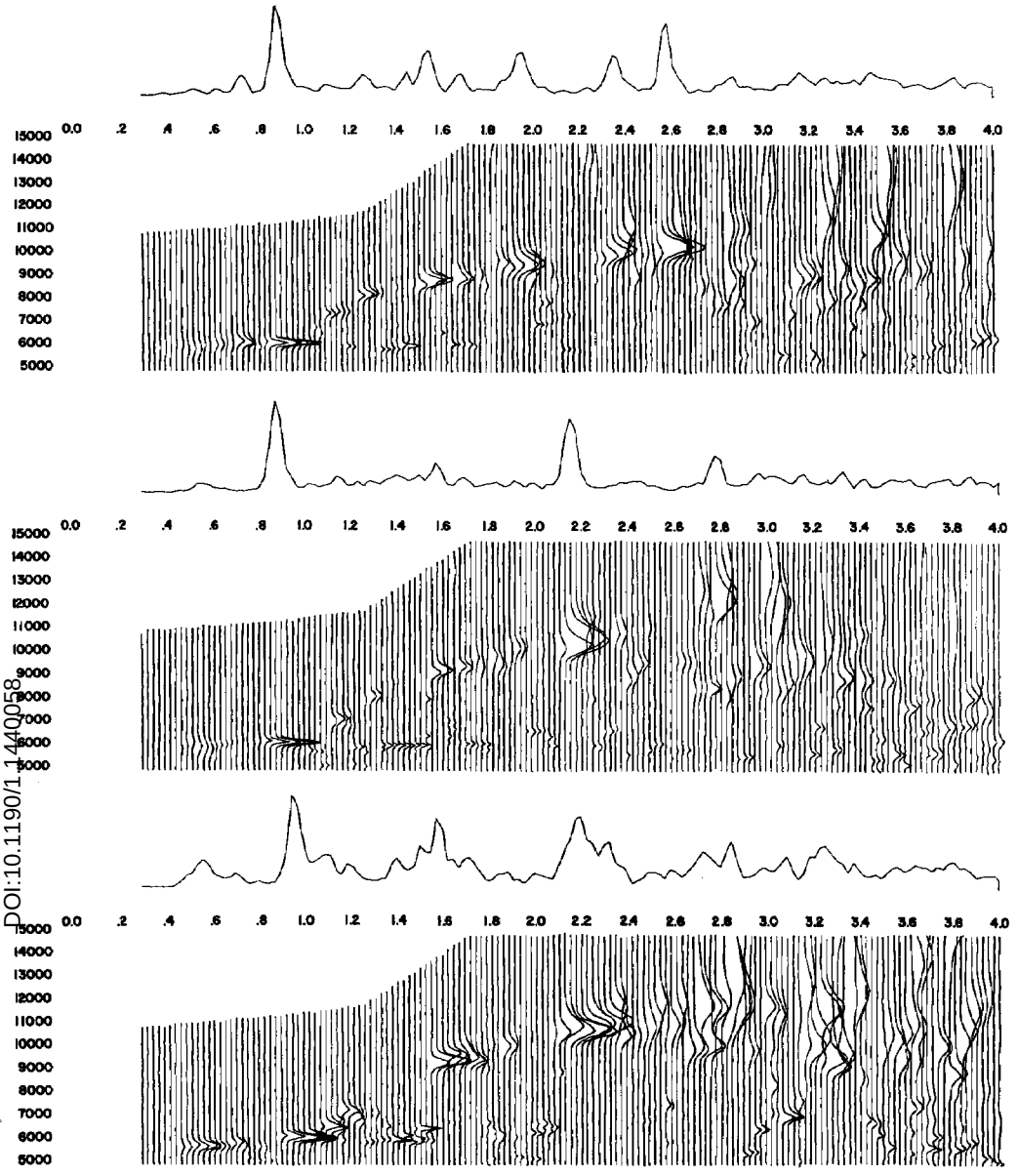

FIG. 13. North Sea velocity spectra displays.

SUMMARY

This paper outlines the fundamental principles for calculating velocity spectra displays. Information about coherent events is derived by means of hyperbolic searches of common reflection point trace gathers. A semblance criterion is used to measure this energy. Where maxima of coherent energy correspond to primary reflections, the display conveniently shows their relation to stacking velocities.

The interpretation of velocity spectra displays is similar to the interpretation of seismic sections in that both should be done by experienced geophysicists. Velocity spectra are an additional tool in the hands of the geophysicist, and they aid him in geophysical as well as geological interpretation

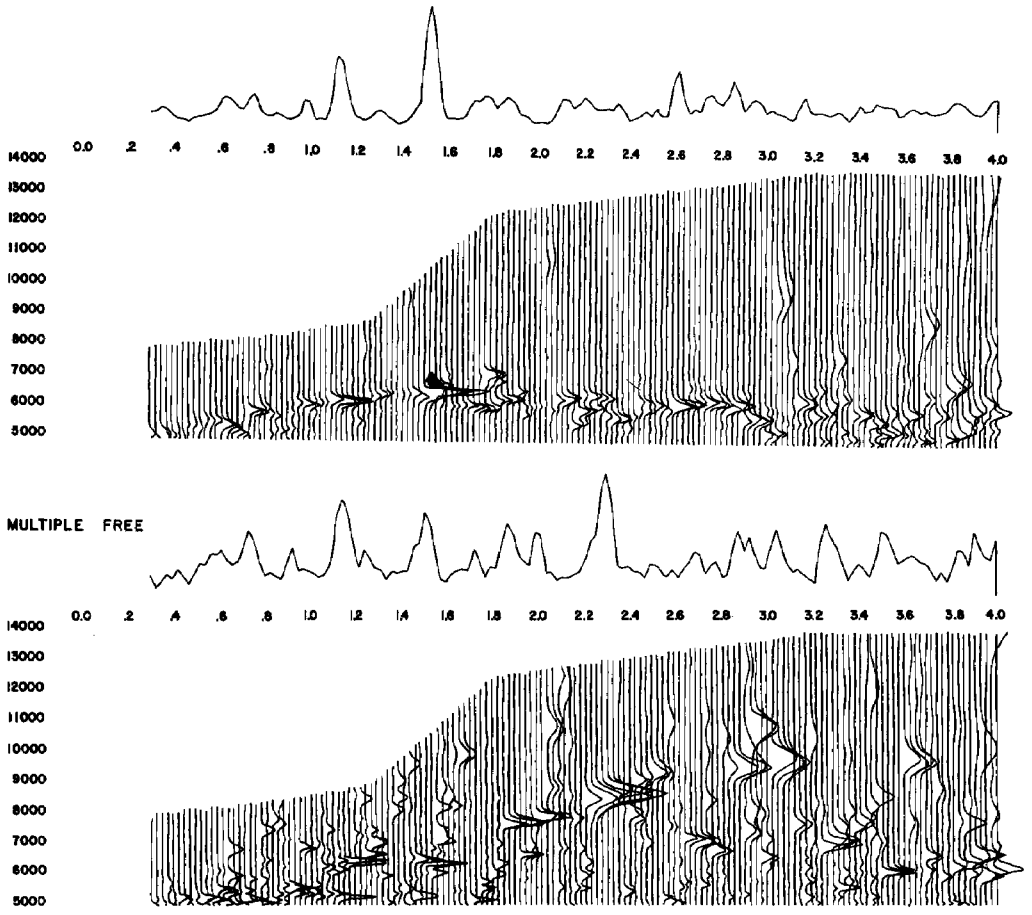

FIG. 14. Velocity spectra displays after multiple suppression. The spectra on the bottom are multiple free.

by allowing him to see his primary reflection events in terms of their velocities. In some cases it was seen that velocity spectra permit character correlations across faults that supplement and confirm those made on the sections. Since the clarity by which the reflections are identified depends on the differential arrival times, a long spread length with single end cable configuration is recommended. Based on the experience gained from velocity spectra, additional interpretational procedures are now being developed to aid the geophysicist in the stratigraphic and structural interpretation.

ACKNOWLEDGMENTS

We would like to take this opportunity to thank Louisiana Land and Exploration Company and Signal Oil and Gas Company for making their data available for presentation in this paper. We would also like to thank Dr. Norman S. Neidell for his comments and his help in the preparation of a final manuscript.

APPENDIX A

TIME-DISTANCE FORMULAS FOR A HORIZONTALLY LAYERED EARTH

Let a coordinate system be chosen with the x axis horizontal and the z axis vertically downward (Figure 1A). Using the method of raypaths, we can compute the time for a ray, starting from the origin, to traverse n horizontal layers, and after reflection return to the surface at the point $(x, 0)$. This is a problem whose solution is well known, being usually found by the use of Snell's law. An alternative method, based on Fermat's principle of least time, is given here.

Let the thicknesses of the n layers be d_1, d_2,

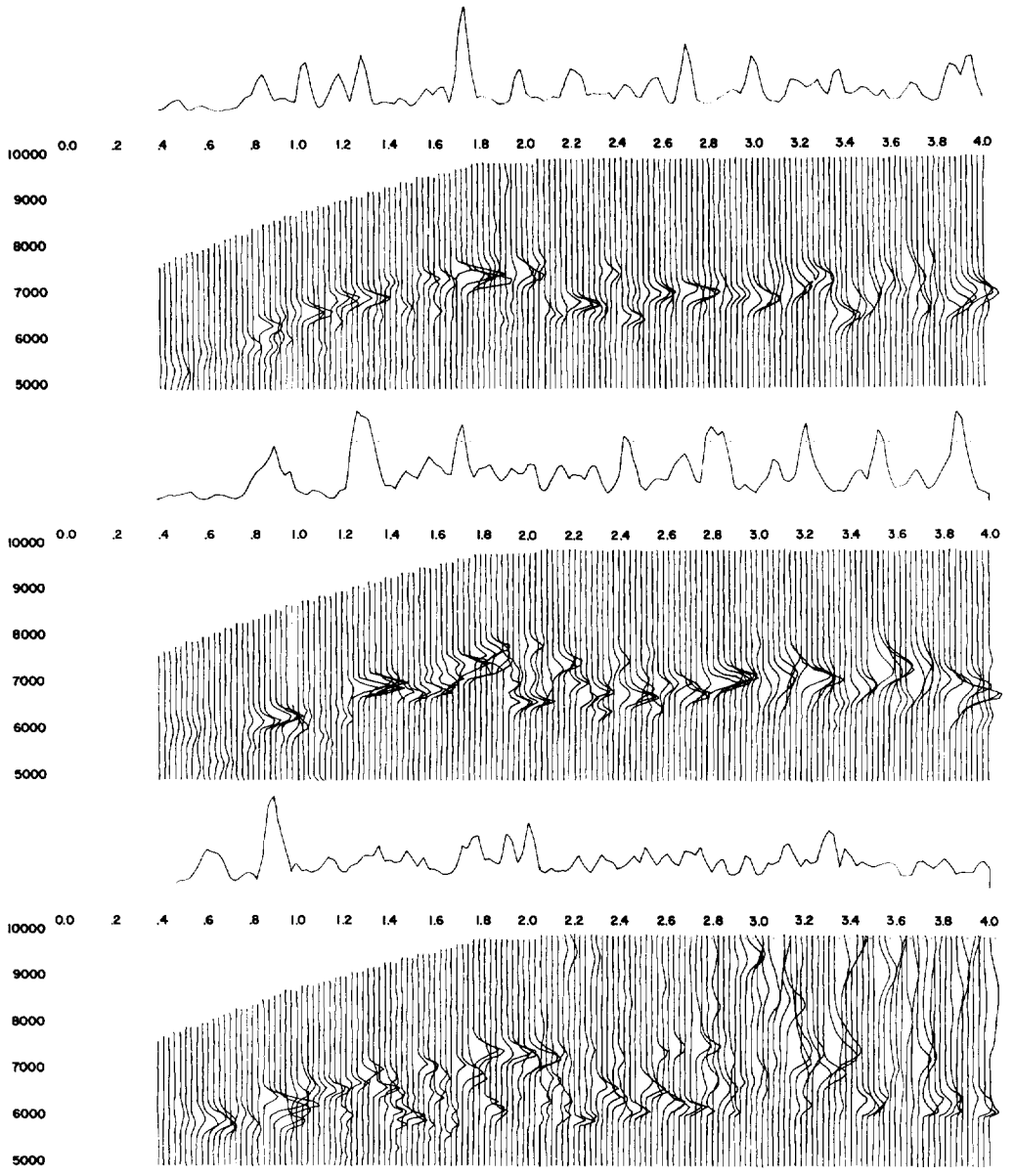

FIG. 15. Velocity spectra displays of velocity inversion.

$d_3, \cdots, d_n$ and the velocities $v_1, v_2, v_3, \cdots, v_n$. The segment of the downward traveling ray within the kth layer will be assumed to have length p_k, with horizontal components x_k and angle to the vertical θ_k as indicated in the figure. The total down-up traveltime T_x is determined, from Fermat's principle and from symmetry about the vertical line through the point of reflection, by the formulas:

$$T_x = 2\sum_{k=1}^{n} \frac{p_k}{v_k} = \text{minimum}, \qquad \text{(A1)}$$

$$p_k^2 = d_k^2 + x_k^2, \qquad \text{(A2)}$$

$$2(x_1 + x_2 + \cdots + x_n) = x. \qquad \text{(A3)}$$

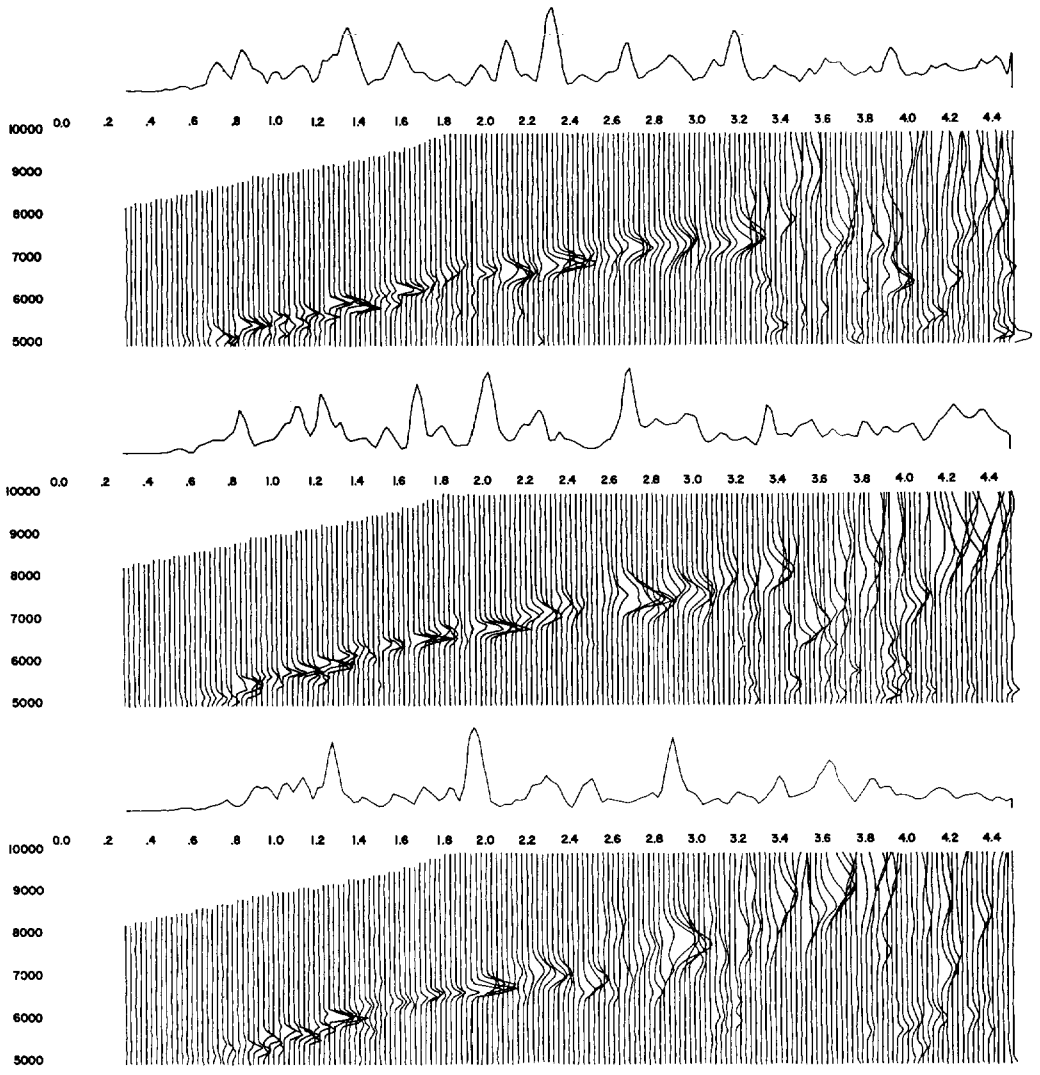

FIG. 16. Velocity spectra displays from gas gun data.

The minimum requirement (A1) under the constraint (A3) leads to the equations,

$$\frac{\delta T_x}{\delta x_k} = \frac{2x_k}{p_k v_k} = 2\lambda, \quad k = 1, 2, \cdots, n \qquad \text{(A4)}$$

where λ is a Lagrange multipler. From (A4) and (A2) we get,

$$x_k^2 = \frac{\lambda^2 v_k^2 d_k^2}{1 - \lambda^2 v_k^2}, \qquad \text{(A5)}$$

and this yields, by substitution in (A3) and (A1),

$$x = 2\lambda \sum_{k=1}^{n} \frac{v_k d_k}{\sqrt{1 - \lambda^2 v_k^2}} \qquad \text{(A6)}$$

$$T_x = 2 \sum_{k=1}^{n} \frac{d_k / v_k}{\sqrt{1 - \lambda^2 v_k^2}}. \qquad \text{(A7)}$$

Equations (A6) and (A7) are the parametric form of the time-distance relationship with λ as parameter as given in Slotnick (1959). As λ varies from 0 to $1/v$, where $v = \max(v_1, v_2, \cdots, v_n)$, x

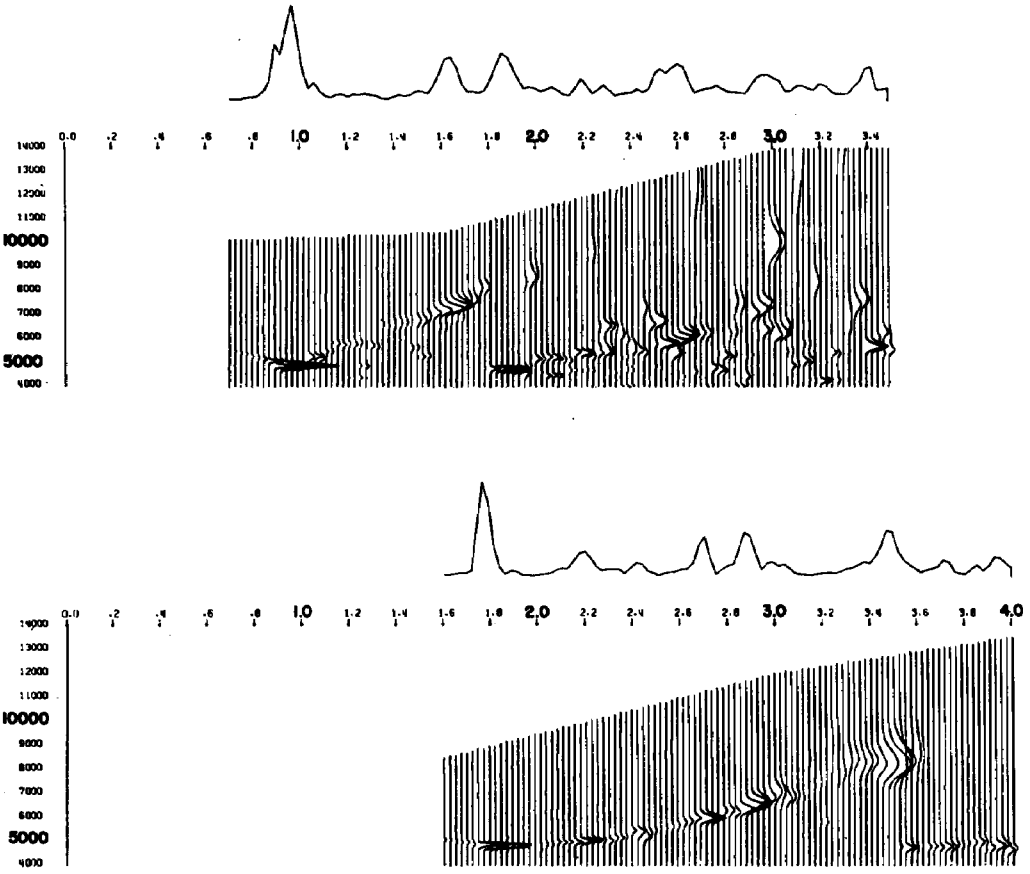

FIG. 17. Velocity spectra displays from marine Vibroseis in the deep sea.

TEST CASE FOR SIMULATOR WITH 6 LAYERS

SHOT POINT = 101

REFLECTOR NO.	TIME	RMS VELO	AVE VELO	INTERVAL VELO	DIP ANGLE	DIP SLOPE	VERT DEPTH	LAYER THICK.	HORIZ DISP.	REFLECTION DEPTH
				5000.				100.		
1	.040	5000.	5000.		.000	.00000	100.		0.	100.
				5999.				1499.		
2	.539	5940.	5925.		2.925	.05109	1599.		-81.	1595.
				7499.				1502.		
3	.925	6736.	6596.		11.368	.20106	3101.		-550.	2991.
				5998.				1000.		
4	1.273	6487.	6439.		.013	.00023	4101.		124.	4101.
				7998.				1000.		
5	1.495	6867.	6695.		-11.390	-.20145	5101.		982.	4903.
				10001.				1595.		
6	1.829	7462.	7267.		-5.649	-.09892	6696.		802.	6617.

FIG. 18. Sample output of interval velocity modeling program.

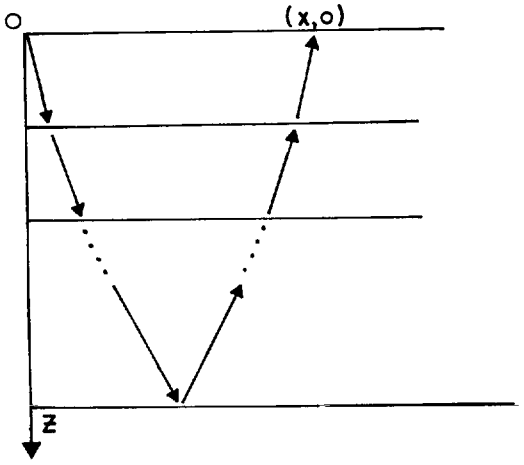

FIG. 1A. Coordinates of a Snell's law raypath in a horizontally layered medium.

will vary from 0 to ∞. The physical significance of the parameter λ can be seen from (A4) and Figure 2A; namely,

$$\lambda = \frac{\sin\theta_k}{v_k}, \quad k = 1, 2, 3, \cdots, n, \quad \text{(A8)}$$

which is Snell's law.

We now consider the problem of deriving an explicit time-distance formula from the parametric equations (A6) and (A7). In the special case where $v_1 = v_2 = \cdots = v_n = v$ these equations reduce to

$$x = \frac{2\lambda v d}{\sqrt{1-\lambda^2 v^2}}, \qquad T_u = \frac{2d}{\sqrt{1-\lambda^2 v^2}}$$

where $d = d_1 + d_2 + \cdots + d_n$, and elimination of λ gives the formula

$$T_x^2 = \frac{4d^2}{v^2} + \frac{x^2}{v^2}. \quad \text{(A9)}$$

From general function-theoretical considerations (Copson, 1935), it can be seen that in the general case there will exist a generalization of the elementary formula (A9) of the form,

$$T_x^2 = c_1 + c_2 x^2 + c_3 x^4 + c_4 x^6 + \cdots \quad \text{(A10)}$$

where the expression on the right-hand side is an infinite series with coefficients c_n which depend on $d_1, d_2, d_3, \cdots, d_n; v_1, v_2, \cdots, v_n$.

The coefficients c_n in (A10) can be expressed by Lagrange's formula or by equivalent contour integrals in the complex plane. A shorter method of computation, however, can be developed using only algebraic operations with power series. The latter method is to express $T_x^2, x^2, x^4, x^6 \cdots$ as a power series in λ^2, derived from (A6) and (A7); substitute these series in (A10); and equate the coefficients of like powers of λ, thus getting a system of equations which can be solved one at a time for $c_1, c_2, c_3 \cdots$. The formulas are as follows: Let

$$q_1 = 1, \quad q_k = \frac{1.\,3.\cdots(2k-3)}{2.\,4.\cdots(2k-2)} \quad (k = 2, 3, \cdots), \quad \text{(A11)}$$

$$a_m = 2\sum_{k=1}^{n} v_k^{2m-3} d_k \quad (m = 1, 2, 3, \cdots), \quad \text{(A12)}$$

$$b_m = q_m a_{m+1} \quad (m = 1, 2, 3, \cdots), \quad \text{(A13)}$$

$$\gamma_m = q_m a_m \quad (m = 1, 2, 3, \cdots). \quad \text{(A14)}$$

From (A6) and (A7) we get

$$x = \sum_{k=1}^{\infty} b_k \lambda^{2k-1}, \quad \text{(A15)}$$

$$T_x = \sum_{k=1}^{\infty} \gamma_k \lambda^{2k-2}. \quad \text{(A16)}$$

Squaring (A15) and (A16), we get

$$x^2 = \lambda^2 \sum_{k=1}^{\infty} B_{k1} \lambda^{2k-2}, \quad \text{(A17)}$$

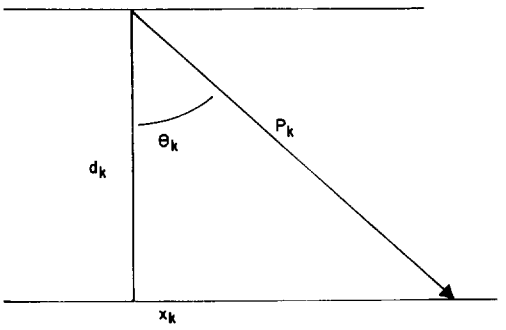

FIG. 2A. Decomposition of a slant path through a layer.

$$T_x^2 = \sum_{k=1}^{\infty} A_k \lambda^{2k-2}, \tag{A18}$$

$$B_{k1} = b_1 b_k + b_2 b_{k-1} + \cdots + b_k b_1, \quad (k = 1, 2, \cdots), \tag{A19}$$

$$A_k = \gamma_1 \gamma_k + \gamma_2 \gamma_{k-1} + \cdots + \gamma_k \gamma_1 \quad (k = 1, 2, \cdots). \tag{A20}$$

From (A17) we can obtain series for x^4, x^6, x^8, $\cdots$.

Let

$$x^{2n} = \lambda^{2n} \sum_{k=1}^{\infty} B_{kn} \lambda^{2k-2} \quad (n = 1, 2, \cdots). \tag{A21}$$

Then the coefficients B_{kn} are determined recursively by

$$B_{kn} = B_{k,n-1} B_{11} + B_{k-1,n-1} B_{21} + B_{1,n-1} B_{k1} \quad \text{for,} \quad (n = 2, 3, 4, \cdots), \quad (k = 1, 2, 3, \cdots). \tag{A22}$$

Substituting (A18) and (A21) in (A10) and equating coefficients gives

$$\begin{aligned} &c_1 = A_1 \\ &c_m B_{1,m-1} + c_{m-1} B_{2,m-2} + \cdots \\ &+ c_2 B_{m-1,1} = A_m \quad (m = 2, 3, 4, \cdots). \end{aligned} \tag{A23}$$

The coefficients $c_1, c_2, c_3, \cdots$ can be computed in recursive fashion from (A23). Explicit formulas for c_1, c_2 are,

$$c_1 = a_1^2 = \left(2 \sum_{k=1}^{n} \frac{d_k}{v_k} \right)^2, \tag{A24}$$

$$c_2 = \frac{a_1}{a_2} = \sum_{k=1}^{n} \frac{d_k}{v_k} \Big/ \sum_{k=1}^{n} v_k k_k. \tag{A25}$$

Let

$$t_k = \frac{d_k}{v_k} = \text{one-way traveltime for a vertical ray to cross the } k\text{th layer.} \tag{A26}$$

It can be seen from (A24) that c_1 is the square of the two-way traveltime for a vertical ray. The reciprocal of c_2 can be written, from (A25) and (A26), as

$$\frac{1}{c_2} = \bar{v} = \frac{\sum_{k=1}^{n} v_k d_k}{\sum_{k=1}^{n} \frac{d_k}{v_k}} = \frac{\sum_{k=1}^{n} t_k v_k^2}{\sum_{k=1}^{n} t_k}. \tag{A27}$$

Hence, $1/c_2$ is the weighted average of the squares of the interval velocities, the weights being equal to the vertical traveltimes. The coefficient $1/v^2$ of the x^2 term in the elementary formula (A9) is thus replaced in the general formula (A10) by the reciprocal of a time-weighted mean square velocity. This same formula is given by Dix (1955).

Formulas for the next three coefficients in (A10) are,

$$c_3 = \frac{a_2^2 - a_1 a_3}{4 a_2^4} \tag{A28}$$

$$c_4 = (2a, a_3^2 - a_1 a_2 a_4 - a_2^2 a_3)/8_a^7 \tag{A29}$$

$$c_5 = \frac{(24 a_1 a_2 a_3 a_4 - 24 a_1 a_3^3 - 5 a_1 a_{2a}^2 + 9 a_2^2 a_3^2 - 4 a_2^3 a_4)}{64 a_2^{10}}. \tag{A30}$$

There does not appear to be any way in general of determining the radius of convergence of the power series (A10). However, in actual cases the numerical results from (A10) and from the parametric formulas (A6) and (A7) can be compared to get some indication of the convergence of (A10). In many cases of practical interest that have been investigated by ourselves and our coworkers, the convergence of (A10) has been found to be quite rapid for all values of x of interest; in fact, so rapid that the first two terms of (A10) give sufficient accuracy for practical purposes in a great many cases.

It is of some interest to note that, when the two-term approximation in (A10) is used, the first neglected term, $c_3 x^4$, is always negative or zero. This follows from (A28) and (A12):

$$A_2^2 = 4\left(\sum_{k=1}^{n} v_k d_k\right)^2$$

$$= 4\left(\sum_{k=1}^{n} \sqrt{v_k^3 d_k}\sqrt{\frac{d_k}{v_k}}\right)^2$$

$$\leq 4\left(\sum_{k=1}^{n} v_k^3 d_k\right)\left(\sum_{k=1}^{n} \frac{d_k}{v_k}\right)$$

by the Schwartz inequality. Hence,

$$a_2^2 = a_1 a_3,$$

$$c_3 \leq 0.$$

The case $c_3=0$ occurs if, and only if, $v_1 = v_2 = \cdots = v_n$.

APPENDIX B

SEMBLANCE AND OTHER COHERENCY CRITERIA

Let us assume that a number of traces $f_i(t)$ $(i=1, 2, \cdots, m)$ corresponding to different values of x, all contain a common signal $S(t)$ from the same reflector but arriving at different times. If the lag times are t_i and if the traces contain only the signal, the lag times can be found theoretically as the solution of a maximization problem.

Let

$$E(\tau_1, \tau_2, \cdots, \tau_m) = \Sigma_t[\Sigma_i f_i(t+\tau_i)]^2. \quad \text{(B1)}$$

Then the maximum of $E(\tau_1, \cdots, \tau_m)$ is attained for $\tau_i = t_i$. For actual traces containing noise in addition to the signal $S(t)$, the criterion of maximizing $E(\tau_1, \cdots, \tau_m)$ can still be used to give an estimate of the arrival times of the coherent signal.

Instead of the function defined in (B1) the sum of the crosscorrelations between pairs of traces with variable lag times can be used; i.e.,

$$C(\tau_1, \tau_2, \cdots, \tau_m) = \Sigma_t \Sigma_{i,j} f_i(t+\tau_i) f_j(t+\tau_j), \quad \text{(B2)}$$

the inner summation being taken over all distinct pairs of different indices (i, j). The E and C functions are connected by

$$2C = E - \Sigma_\tau \Sigma_i f_i^2(t). \quad \text{(B3)}$$

A normalized form of the E function called the semblance would be:

$$P(\tau_1, \tau_2, \cdots, \tau_m) = \frac{E}{m\Sigma_t \Sigma_i f_i^2(t)} \quad \text{(B4)}$$

which has a possible range from 0 to 1. Such a normalized function, the semblance coefficient, gives a measure of coherency which is, in a sense, independent of the joint power level of the traces. More precisely, the P function is unchanged when a set of traces $f_i(t)$ is replaced by a set $kf_i(t)$, for any value of the scale factor k. It is, however, sensitive to the variations within the set of traces, unlike normalized crosscorrelation.

The maximization of any of the functions E, C, P when m is equal to, say 6, presents a numerical problem of considerable magnitude and can be solved only by a long sequence of successive approximations. The problem is greatly simplified if it can be assumed that the lag times depend on only one or two parameters.

For applications in identifying velocities, the simplest assumption is based on the two-term approximation to (A10) with a selected value for c_1 of $T_{0,n}^2$ and with c_2 being $(1/\overline{V}^2)$ where,

$T_{0,n}$ = two-way normal incidence traveltime [see (1) and (A24)]

$\overline{V}$ = time-weighted mean square velocity [see (7) and (A27)]

In this case it is a relatively simple matter to compute the value of E (or, C, or P) as a function of $\overline{V}$ and to pick the value of $\overline{V}$ which gives the maximum.

If the x values in (A10) are so large that the two term approximation is too crude, or if account is to be taken of sloping interfaces in a single coverage trace gather, the lag times t_i must be assumed to depend on more than two parameters. With sloping interfaces the formula for τ^2, analogous to (A10), will contain odd powers of x as well as even ones.

REFERENCES

Cook, E. E., 1967, Geophysical reconnaissance in the Northwestern Caribbean: Presented at the 37th Annual International S.E.G. Meeting, October 31, 1968, Oklahoma City, Oklahoma.

Copson, C. T., 1935, Theory of functions of a complex variable: Oxford University Press, p. 121–125.

Courtier, W. H., and Mendenhall, H. L., 1967, Experiences with multiple coverage seismic methods: Geophysics, v. 32, p. 230–258.

Dix, C. H., 1955, Seismic velocities from surface measurements: Geophysics, v. 20, p. 68–86.
Mayne, W. H., 1962, Common reflection point horizontal stacking techniques: Geophysics, v. 27, p. 927–938.
——— 1967, Practical considerations in the use of common reflection point techniques: Geophysics, v. 32, p. 225–229.
Nugent, L. E., Jr., 1965, Critical analysis of stack seismic systems: Bull. Amer. Assoc. Petrol. Geol., v. 51, p. 915–956.
Picon, C., and Utzmann, R., 1962, La "Coupe sismique vectorielle" un pointé semi-automatique: Geophys. Prosp., v. 10, p. 497–516.
Rieber, F., 1936, A new reflection system with controlled directional sensitivity: Geophysics, v. 1, p. 97–106.
Sattlegger, J., 1965, A method of computing interval velocities from expanding spread data in the case of arbitrary long spreads and arbitrarily dipping interfaces: Geophys. Prosp., v. 13, p. 306–318.
Schneider, W. A., and Backus, M., 1968, Dynamic correlation analysis: Geophysics, v. 33, p. 105–126.
Simpson, J. K., 1967, Traveling signal-to-noise ratio and signal power estimates: Geophysics, v. 32, p. 485–493.
Slotnick, M. M., 1959, Lessons in seismic computing: Tulsa, SEG, p. 194.
Trorey, A. W., 1961, The information content of a Rieber Sonogram: Geophysics, v. 26, p. 761–764.